Kinetochore-independent sister chromosome separation is driven by plus-end microtubule dynamics

Hannah Vicars[1]*, Travis Karg[1], Brandt Warecki[1], Ian Bast[1], William Sullivan[1].

[1] Department of Molecular, Cell and Developmental Biology, University of California, Santa Cruz, Santa Cruz, CA, USA

*Email: hvicars@ucsc.edu (HV)

Author contributions: HV contributed to all aspects of planning, execution of the experiments, analysis, and manuscript preparation. TK contributed to the planning, execution, and analysis of the RNAi screen and the planning and execution of live imaging of greatwall hypomorphs. BW contributed to the planning, execution, and analysis of the telomere-labeling experiments. IB contributed to the execution and analysis of the telomere-labeling experiments. WS contributed to all aspects of experimental planning and manuscript preparation.

ABSTRACT

Although centromeres play a key role in sister chromatid separation and segregation, mitotic transmission of chromosome fragments lacking a centromere (acentrics) can be successful. In *Drosophila* neuroblasts, acentric chromosomes undergo delayed, but successful transmission revealing the existence of kinetochore-independent mechanisms driving transmission. In spite of delayed sister chromatid separation, bulk cohesin removal from the acentric is not delayed, suggesting factors other than cohesin are responsible for the delay. In contrast to intact kinetochore-bearing chromosomes, we discovered that acentrics align parallel as well as perpendicular to the mitotic spindle. In addition, sister acentrics undergo unconventional patterns of separation. For example, rather than the simultaneous separation of sisters, acentrics oriented parallel to the spindle often slide past one another toward opposing poles. To identify the mechanisms driving acentric separation, we screened 117 RNAi gene knockdowns for synthetic lethality with acentric chromosome fragments. In addition to well-established DNA repair and checkpoint mutants, this candidate screen identified synthetic lethality with X-chromosome-derived acentric fragments in knockdowns of Greatwall (cell cycle kinase), EB1 (plus-end tracking protein), and Map205 (microtubule-stabilizing protein). Additional image-based screening revealed that reductions in Topoisomerase II levels disrupted sister acentric separation. Intriguingly, live imaging revealed that knockdowns of EB1, Map205, and Greatwall preferentially disrupted the sliding mode of sister acentric separation. In spite of these failures in acentric separation, acentrics incorporated into daughter nuclei and there was no increase in micronuclei formation. Based on our analysis of EB1 localization and knockdown phenotypes, we propose that in the absence of a kinetochore, microtubule plus-end dynamics provide the force to resolve DNA catenations required for sister separation.

AUTHOR SUMMARY

Centromeres, the site on the chromosomes to which microtubules attach driving the separation and segregation of replicated sister chromosomes, have been viewed as essential for proper cell division and accurate transmission of chromosomes into daughter cells. However previous studies demonstrated that sister chromosomes lacking a centromere (acentrics) often undergo separation, segregation and transmission. Here we demonstrate that sister acentrics are held together through DNA intertwining. During anaphase, acentric sister separation is achieved through Topoisomerase activity, an enzyme that resolves these DNA linkages, as well as forces generated on the acentrics by the growing ends of highly dynamic microtubule polymers. We found acentric sister chromatids display unique patterns of separation using mechanisms independent of the centromere. Additionally, we identified the specific microtubule-associated proteins required for the successful mitotic transmission of acentric chromosomes to daughter cells. These studies reveal unsuspected, distinct forces that likely act on all chromosomes during mitosis independent of centromere-microtubule attachments.

INTRODUCTION

Eukaryotic cells have evolved mechanisms to detect and protect against genomic insults. These mechanisms include checkpoint pathways that delay cell cycle progression allowing time for repair and apoptotic pathways that eliminate the damaged cells from the dividing population [1]. Although a great deal is known regarding the function of these corrective pathways during interphase, much less is known about the mechanisms that protect against genomic instability after exit from metaphase. Studies demonstrate that DNA damage persisting through metaphase delays anaphase onset. This delay is mediated both by the DNA damage and spindle assembly checkpoint pathways [2, 3].

52 Despite these mechanisms, if the DNA damage remains, the checkpoints are overridden,
53 and the cell exits metaphase [4]. The persistence of unrepaired double-strand breaks (DSBs) at
54 metaphase is particularly problematic due to the formation of chromosome fragments, one of
55 which lacks a telomere and the other lacking a centromere and a telomere. The latter are known
56 as acentrics and are incapable of forming canonical microtubule-kinetochore attachments that
57 drive poleward chromosome segregation. Consequently, acentrics would be expected to lag on
58 the metaphase plate and exhibit severe segregation defects. In accord with this expectation,
59 acentrics often fail to segregate, are excluded from daughter nuclei, and subsequently form
60 cytoplasmic micronuclei [5-7]. However, a growing number of reports demonstrate poleward
61 migration of acentric chromosome fragments [5, 8-13]. Proposed mechanisms of acentric
62 segregation include neo-centromere formation [14] and direct association of the acentric
63 chromosome with microtubules [15] or a kinetochore-bearing chromosome [16-18].

64 Acentrics are efficiently generated in *Drosophila* bearing an I-CreI endonuclease
65 transgene, which fortuitously recognizes a repetitive sequence within the pericentric rDNA repeats
66 of the *Drosophila* X chromosome [19-22]. Induction of I-CreI expression results in the formation
67 of acentrics in over 80% of third instar larval neuroblast cells [12]. Although acentrics lag behind
68 on the metaphase plate well after the intact chromosomes migrate toward opposite poles, the
69 acentrics have a remarkable ability to accurately separate, segregate and incorporate into
70 daughter telophase nuclei. Acentric segregation relies on the chromokinesin Klp3A and interpolar
71 microtubules [15]. Sister acentrics are held together on the metaphase plate well after the main
72 chromosome mass has segregated, suggesting the existence of kinetochore-independent
73 mechanisms for maintaining sister chromosome association on the metaphase plate and delaying
74 their separation during anaphase. Possible explanations include delayed acentric cohesin
75 removal, delayed resolution of sister DNA catenations, or opposing plus-end directed microtubule
76 forces acting on each sister.

Here we employ a combination of synthetic lethal screens and live imaging to identify factors required for proper separation of sister acentrics. Live analysis reveals three distinct modes of acentric separation: unzipping, sliding, and dissociation. This candidate screen revealed that Topoisomerase II, the cell-cycle regulator Greatwall kinase, the microtubule (MT) plus-end tracking protein EB1, and the MT-associated protein Map205 provide key roles in sister separation of acentrics. In addition, gene knockdowns of EB1, Map205, and Greatwall preferentially disrupt the sliding mode of sister separation. As will be discussed, this analysis demonstrates the existence of kinetochore-independent mechanisms facilitating sister chromosome separation.

RESULTS

Acentric sister separation, but not cohesin removal, is delayed during the metaphase-to-anaphase transition

As described previously, acentric chromosome fragments are efficiently generated through heat-shock induction of an I-CreI transgene that specifically targets and creates DSBs in the rDNA repeats at the base of the *Drosophila* X chromosome [19]. In accord with previous studies [12], live analysis of the resulting X chromosome acentrics in the larval neuroblasts reveals that sister separation of the acentrics occurs on average 100 seconds (± 48, n=19) after segregation of the intact chromosomes (**Figure 1, Table 1**). Sister chromatids are held together at metaphase by cohesin, a tripartite ring-like protein complex comprised of two structural maintenance of chromosome proteins (SMC1, SMC3) and a kleisin subunit (Rad21/Scc1) [23, 24]. Initially, cohesin removal occurs only along the chromosome arms through proteolytic cleavage of the kleisin subunit by separase just prior to anaphase onset [25-27]. Due to the

103 Sgo/PP2A-dependent protection mechanism, cohesin remains at the centromeric regions [28].
104 Once removed, microtubules drive sister separation [29]. The delay in cohesin removal does not
105 depend on proximity to the centromere, as it occurs in chromosome rearrangements in which the
106 centric heterochromatin is no longer associated with the centromere [30].

107 To investigate if delays in cohesin release are responsible for the delayed separation of
108 acentric chromosomes, female neuroblast divisions were live imaged with a cohesin component,
109 Rad21, tagged with EGFP [31]. Time-lapse images of a control neuroblast expressing Rad21-
110 EGFP are shown in **Figure 2A** (chromosomes in magenta, cohesin in green). No lagging
111 chromosomes are observed and Rad21 is cleared off of all chromosomes just prior to anaphase
112 onset and separation of sister chromatids. **Figure 2B and Supplemental Movie 1** show time-
113 lapse images of an I-CreI-expressing neuroblast division. Separation and segregation of sister
114 acentrics is delayed relative to the intact chromosomes. However, cohesin removal just prior to
115 anaphase onset from the acentrics and the intact kinetochore-bearing chromosomes occurs
116 simultaneously. This is more clearly seen in the single channel black and white cohesin images
117 of **Figure 2B** (depicting yellow outlined regions of **Figure 2B**). Quantification of the Rad21
118 fluorescent signal supports the conclusion of a relatively synchronous removal of cohesin on the
119 acentric and intact chromosomes (**Figure 2C**).

120 The finding that sister acentrics remain paired despite the absence of cohesin and well
121 after the intact chromosomes have separated, indicate additional forces hold sister acentrics
122 together.

123

124 **Acentric sister separation occurs via three distinct patterns**

125

126 To examine dynamics of acentric separation, we imaged live neuroblasts expressing I-
127 CreI, the histone marker H2Av-RFP, and the telomere marker HOAP-GFP [32]. Marked telomeres

128 enabled us to determine the orientation of acentrics with respect to one another as they aligned
129 on the metaphase plate, separated, and segregated poleward [15]. We observed three distinct
130 patterns of sister acentric separation (**Figure 3**). In the most frequent pattern (49%, N=45),
131 acentric pairs separate by sliding past one another (**Figure 3A**, Top row: histone-labeled
132 chromosomes in magenta, HOAP-labeled telomeres in green). This is more clearly observed in
133 the single histone channel movie (**Figure 3A Bottom row and Supplemental Movie 2**). In
134 contrast to intact kinetochore-bearing chromosomes which always align perpendicular to the
135 spindle, the paired sister acentrics align either parallel or perpendicular to the spindle and division
136 axis. Later, the separation and segregation of sisters toward opposite poles always occurs with
137 the acentrics aligned parallel to the spindle.

138 The second pattern of acentric separation occurs via an "unzipping" mechanism (**Figure**
139 **3B**). This pattern occurs at a frequency of 31% (N=45). During separation, sister acentrics often
140 first separate at the broken end followed by separation at the telomere. This is illustrated in **Figure**
141 **3B**: the telomeres remain associated while the broken ends are well separated. Rarely, the paired
142 acentrics unzip from the telomere end first. In contrast to the acentrics that separate by sliding,
143 these paired sister acentrics are usually aligned perpendicular to the spindle and division axis.

144 In the third pattern of separation, the remaining 20% (N=45), acentric sisters cleanly
145 separate from one another along their entire length similar to that observed for centric
146 chromosomes (**Figure 3C**). We termed this centric-like pattern: dissociation. Acentrics that
147 separate via dissociation are aligned in multiple orientations on the metaphase plate (from parallel
148 to perpendicular) with respect to the spindle and division axis. At separation, dissociating sister
149 acentrics simultaneously separate along their entire lengths.

150 We next analyzed the orientation of sister acentrics with respect to one another at the time
151 of separation through labeling telomeres with HOAP-GFP. As expected, the vast majority (87%,
152 39/45) of sister acentrics were oriented with their telomeres paired and aligned (**Figure 3D**).
153 However, a small but notable fraction (13%, 6/45), aligned with their telomeres opposed (**Figure**

154 **3D**). Acentric pairs that align with telomeres opposed presumably have already lost catenation
155 and/or cohesin in order to adopt this geometry. 14% and 33% of acentric sisters that separated
156 by sliding and dissociating, respectively, aligned with their telomeres opposed. Interestingly, sister
157 acentrics that separated by unzipping were never observed aligned with their telomeres opposed.
158 This suggests that there is an absolute requirement for sister pairing in acentrics that separate by
159 unzipping.

160 To further characterize these three modes of acentric separation, we measured the time
161 from anaphase onset (as determined by separation of the intact chromosomes) to sister acentric
162 separation (**Figure 3E**). Sliding acentrics separated much later than acentrics (202 ± 51 seconds)
163 that separated either by unzipping (131 ± 54 seconds) or dissociating (106 ± 55 seconds) (N=45,
164 **Figure 3E**). These differences were statistically significant as determined by two-sided Mann-
165 Whitney tests (p=0.0008 and p=0.0008, respectively). We did not detect any difference in the
166 timing of acentric sister separation by unzipping or dissociating (p=0.25 as determined by a two-
167 tailed Mann-Whitney test).

168 Taken together, these results demonstrate three distinct patterns for acentric separation.
169 We note that based on the movements and orientation of both sliding and dissociating acentrics,
170 it is possible that catenation must be lost along the entire length of the acentric pair simultaneously
171 at the moment of separation. In contrast, acentrics that separate by unzipping and appear to have
172 an absolute requirement for sister pairing may be more tightly associated with one another, and
173 this tight association may be due to lingering catenations.

174

175 **Synthetic lethal screen identifies genes required for separation of sister acentrics**

176

177 To identify the mechanisms required for transmission of acentric sister chromosomes, we
178 screened candidate RNAi gene knockdowns for those that resulted in synthetic lethality in the

179 presence of acentrics. The rationale for this screen is based on previous studies demonstrating
180 that I-CreI induction of acentric chromosomes during third instar larval stage resulted in only slight
181 reductions in adult survival because the acentrics are efficiently transmitted to daughter nuclei
182 [12]. However, reducing or partially disrupting the function of genes required for the normal
183 acentric transmission results in a dramatic reduction in adult survival upon acentric induction [12,
184 15]. Thus, we expected that a subset of the gene knockdowns that resulted in synthetic lethality
185 upon I-CreI induction would be required for proper pairing and segregation of sister acentrics.

186 To perform the screen, adult flies bearing a heat-shock inducible I-CreI endonuclease and
187 Gal4 under the control of a ubiquitously expressed Actin enhancer element (Act5) were crossed
188 to adults bearing UAS-gene specific RNAi constructs. Lethality of heat-shocked (I-CreI induced)
189 and non-heat-shocked (I-CreI not induced) F1 progeny bearing both constructs were assayed.
190 RNAi constructs that significantly increased lethality upon I-CreI induction were of particular
191 interest. We screened 117 candidate genes for synthetic lethality upon acentric induction
192 (**Supplemental Table 1**). These included genes encoding proteins spanning a diversity of mitotic
193 functions, including microtubule-associated proteins, chromatin remodelers, DNA repair genes,
194 cell cycle kinases, and cell cycle checkpoints. For each RNAi line, we determined the survival
195 ratio of the RNAi knockdown with I-CreI induced to the RNAi knockdown alone ([RNAi knockdown
196 + I-CreI]/[RNAi knockdown]). A ratio of less than 0.65 was scored as a significant synthetic lethal
197 interaction (**Table 2**).

198 The acentrics are generated through I-CreI induced double-strand breaks. As expected,
199 RNAi knockdowns of DNA repair and cell cycle checkpoints exhibit synthetic lethality upon I-CreI
200 induction. Genes involved in DNA repair (*spnA/Rad51*, DSB repair [33]; *mus309*, DSB repair [34];
201 and *Ku80*, NHEJ [35]) all exhibit strong synthetic lethality upon I-CreI induction with survival ratios
202 of 2%, 11%, and 29%, respectively (**Table 2**). The DNA damage checkpoint gene *tefu* (ATM [36])
203 also results in a pronounced synthetic lethality (survival ratio of 43%).

204 The screen also yielded a number of microtubule-associated proteins. These included
205 *msps* (microtubule nucleation [37]), *asp* (astral microtubule organization [38]), *eb1* (plus-end
206 microtubule binding [39]), *klp68D* (kinesin motor protein [40]), and *map205* (microtubule stabilizer
207 [41]). Given that microtubule-based transport plays a key role in the poleward transport of the
208 acentric chromosome fragments [15], synthetic lethal interactions with microtubule-associated
209 proteins were expected.

210 The screen also yielded a large class of genes involved in chromatin organization. This
211 included *cap-D2* (condensin [42]), *chd1* (ATP-dependent chromatin remodeler [43]), *sin3A* and
212 *sir2* (histone deacetylases [44]), *chrac* (nucleosome mobilization [45]), and *hp1* (heterochromatin
213 protein [46]). Whether these are directly required for double-strand break repair, separation and/or
214 segregation of sister acentrics remains to be determined.

215 In accord with previous work, reduced levels of BubR1 kinase (spindle-assembly
216 checkpoint protein) also exhibited a pronounced synthetic lethality upon I-CreI induction [12]. The
217 screen also yielded two additional cell cycle kinases: *gwl* (greatwall kinase, an inhibitor of the cell
218 cycle phosphatase PP2A [47]) and *ald* (altered disjunction, chromosome segregation [48]).

219

220 **Live imaging analysis reveals the microtubule-associated proteins Map205 and EB1 and**
221 **Topo II are required for separation, but not segregation of sister acentrics.**

222

223 We conducted live imaging experiments on neuroblasts to investigate the effect of specific
224 RNAi-mediated gene knockdowns on acentric mitotic transmission. Each line contains an RFP-
225 tagged histone transgene facilitating live confocal analysis [49]. Based on previous studies
226 revealing the role of microtubules in acentric transmission [15], we initially focused on the
227 microtubule-stabilizing protein Map205 and the microtubule plus-end associated protein EB1.

228 In a wild-type background, the majority of acentrics line up at the outer edge of the
229 metaphase plate, separated from the main mass of intact chromosomes [12, 15]. As described
230 above and in previous publications, during anaphase sister acentrics remain paired on the
231 metaphase plate well after the separation of intact chromosomes (**Figure 4A**) [12, 15]. On
232 average, separation of sister acentrics occurs 100 seconds ± 48 (N=19) after separation of the
233 kinetochore-bearing chromosomes (**Table 1**). 83% (19/23) of acentric sister chromatid pairs
234 separate normally with sister acentrics going to opposite cell poles (**Figure 4C**). In the remaining
235 17% (4/23), acentric sister chromatids line up in metaphase, lag behind at the metaphase plate,
236 and segregate together to one pole of the cell. Micronuclei form in telophase in 24% (4/17) of
237 neuroblasts expressing I-CreI micronuclei form in telophase (**Figure 4D**).

238 Live imaging of acentric behavior in neuroblasts expressing Map205 RNAi revealed that
239 47% (8/17) of acentric sister chromatids do not separate from one another and segregate to one
240 cell pole together, in comparison to 17% (4/23) in a wildtype background (**Figure 4C, Figure 5B**).
241 In spite of defects in sister chromatid separation, the timing of the initiation of poleward
242 segregation and their poleward segregation rate were normal (**Figure 5D, Table 3**). Despite the
243 increase in failed acentric separation, there was not an increase in micronuclei formation (9%
244 compared to 24% in controls) (**Figure 4D**).

245 Live analysis of acentric behavior in neuroblasts expressing EB1 RNAi revealed that 47%
246 (14/30) of acentric sister pairs fail to separate (**Figure 4C, Figure 5E**). The failure of separation
247 results in acentric sisters segregating together to a single cell pole (**Figure 4B and Supplemental**
248 **Movie 3**). Similarly, to the cells with Map205 knockdown, the timing of acentric segregation
249 initiation and their rate of poleward segregation was normal (**Figure 5E, Table 3**). There was also
250 not an increase in micronuclei formation (8% compared to 24% in controls) (**Figure 4D**). This
251 indicates that the Map205 and EB1 knockdowns are specifically disrupting sister separation of
252 acentrics and have no effect on the latter stages of acentric transmission.

253 As described earlier, cohesin removal on the intact chromosomes and acentrics occurs
254 simultaneously, yet acentric sisters remain paired. This raised the possibility of a role for DNA
255 catenation in maintaining acentric pairing. Previous work demonstrated that DNA catenations
256 preserve sister chromatid cohesion in intact chromosomes until resolution by Topoisomerase II
257 (Topo II) at the metaphase-anaphase transition [50]. Topo II decatenates intertwined DNA
258 allowing sister chromatids to segregate to opposing poles of the cell. To test the role of DNA
259 catenation in maintaining acentric sister pairing, we knocked down levels of Topo II specifically in
260 the *Drosophila* neuroblast using the Gal4/UAS RNAi technique described above. Topo II
261 knockdowns revealed that 50% (8/16) of sister acentrics fail to separate and subsequently
262 segregate together to one pole (**Figure 6 and Supplemental Movie 4**). Due to the lasting
263 catenations between acentric sisters, the timing of initiation of acentric separation was further
264 delayed in neuroblasts expressing Topo II RNAi (t-test; $p = 0.04$) (**Table 1**). Although acentric
265 separation is disrupted, their poleward segregation rate and their rate of micronuclei formation
266 were normal (**Figure 5F, Table 3, Figure 4D**).
267 The screen also yielded the PP2A inhibitor Greatwall kinase (*gwl*) that controls the timing
268 and events of mitotic exit including sister chromatid separation [51]. Thus, we were particularly
269 interested in the dynamics of acentric separation and segregation when the levels of *gwl* were
270 reduced. This analysis uncovered that with reduced levels of *gwl*, 39% (14/36) of acentric sister
271 pairs failed to separate from one another (**Figure 4C, Figure 5B**). Additionally, the timing of the
272 initiation of poleward segregation, the rate of poleward segregation, and the rate of micronuclei
273 formation were normal (**Figure 5G, Table 3, Figure 4D**).
274
275 **EB1, Map205, Greatwall, and Topo II differentially influence the dynamics of acentric**
276 **separation**
277

278 As described above, in a wild-type background acentrics exhibit three distinct patterns of
279 separation: sliding, unzipping, and dissociation. Sliding is the most frequent occurring 49% of the
280 time, with unzipping and dissociation occurring at frequencies of 31% and 20%, respectively
281 (**Figure 3E**). To determine the role of the genes identified above in these distinct forms of acentric
282 separation, we monitored the frequency of segregation patterns in RNAi knockdowns of the
283 candidate genes. RNAi knockdowns of Map205 and Greatwall decreased the frequency of
284 separation via sliding. Additionally, RNAi knockdown of Topoisomerase II decreased the
285 frequency of separation by sliding as well as unzipping. Similarly, RNAi knockdowns of EB1
286 resulted in a dramatic decrease in the frequency of acentric separation by sliding (**Figure 5B**).
287 To determine if microtubule plus-ends preferentially accumulate around acentrics, I-CreI-
288 expressing neuroblasts were live imaged with EGFP-tagged EB1. Fluorescence intensities of both
289 GFP and RFP were measured and corrected for brightness in control neuroblasts (N=5) and I-
290 CreI-expressing neuroblasts (N=5). During mitosis, EB1 localizes along microtubules moving
291 towards the plus-ends (**Figure 7 and Supplemental Movie 5**). It was previously demonstrated
292 that acentrics are surrounded by microtubules during anaphase [15], consequently EB1
293 associates with these microtubules and surrounds acentrics. However, the concentration of EB1
294 is not significantly increased at or near the acentrics ($P > 0.05$, two sample t-test; **Figure 7**). Thus,
295 while EB1 and the acentrics co-localize, we do not observe a preferential recruitment and
296 accumulation of this protein at the microtubule plus-ends.
297
298 **DISCUSSION**
299
300 Although much of chromosome dynamics is driven by the kinetochore, numerous studies
301 reveal additional forces act on the chromosomes during mitosis [52]. Here we focused on the role
302 of kinetochore independent forces driving sister chromatid separation. A key finding is that while
303 cohesin removal occurs simultaneously on intact and acentric chromosomes, sister separation of

304 the latter is significantly delayed. An explanation for this delay comes from studies of intact
305 chromosomes demonstrating that once cohesin is removed, sister acentrics remain held together
306 through DNA catenations [50, 53, 54].

307 Catenations are concentrated at the centromeric DNA and opposing kinetochore
308 microtubule interactions likely provide the resolving force [55-59]. Support for this conclusion
309 comes from studies of chromosome rearrangements in which centromeric heterochromatin is
310 displaced from the centromere [30]. Sister chromatin separation is specifically delayed in these
311 regions resulting in localized stretching during anaphase. A likely consequence of being displaced
312 from the centromere is that the ectopic heterochromatic regions no longer experience sufficient
313 kinetochore forces required to efficiently resolve sister DNA catenations. In light of these studies,
314 it is likely that acentric sisters remain associated well after separation of the intact chromosomes
315 through DNA catenations. This conclusion is supported by our finding that reductions in the
316 Topoisomerase II levels specifically disrupt acentric sister separation. As described below, our
317 studies suggest both plus-end and lateral microtubule interactions with the acentrics provide the
318 alternative force driving sister separation.

319 Intact chromosomes align perpendicular to the spindle. In contrast, we find acentric
320 chromosomes align either perpendicular or parallel to the spindle. Without a kinetochore, a
321 combination of lateral and plus-end microtubule interactions likely determines the final orientation
322 of acentrics on the metaphase plate. In addition to the multiple orientations, acentrics undergo
323 distinct patterns of sister separation that we have termed sliding, unzipping and dissociation.
324 Sliding of sisters past one another toward opposite poles is the most common mode of acentric
325 separation. This mode occurs primarily when sister acentrics are oriented parallel to the spindle
326 just prior to separation suggesting lateral microtubule interactions provide the force driving this
327 mode of acentric separation (**Figure 3A, Figure 5C, Table 4**). While sister separation of all
328 acentrics is delayed relative to intact chromosomes, the delay is much more pronounced for
329 acentrics that undergo separation by sliding. The delay may in part be due to the additional time

330 it takes to establish the multiple lateral interactions required to generate sufficient separation
331 force. It is likely chromokinesins provide the force driving separation, but these have yet to be
332 identified.

333 In contrast to sliding, sister separation by unzipping occurs primarily when the acentrics
334 are oriented perpendicular to the spindle just prior to separation suggesting a limited role for lateral
335 microtubule interactions (**Figure 3B, Figure 5C, Table 4**). During unzipping, acentrics generally
336 initiate separation at their broken ends with completion of separation occurring at the telomeres.
337 The delay of acentric separation by unzipping is much less than the delay observed for separation
338 by sliding. Previous studies demonstrated that the acentric and its centric partner are connected
339 via a DNA tether [12]. The preference for initiation of separation at the broken-ends suggests that
340 a DNA tether connecting the broken end to the centromere-bearing fragment may provide the
341 initial separation force (**Figure 3B**). While this tether is not thought to provide the force driving
342 acentric separation, because of its association with the broken end of the acentric, it may drive
343 the initial stage of unzipping. In contrast to separation by sliding, telomeres are always aligned in
344 sisters that separate by unzipping (**Figure 3E, Figure 3F**). This suggests maintaining gene-for-
345 gene sister pairing is essential for this form of separation.

346 The third mode of acentric separation, dissociation, is characterized by a simultaneous
347 separation along the entire length of sister acentrics (**Figure 3C**). While sister separation via
348 dissociation favors the perpendicular orientation, this skewing is much less dramatic compared to
349 the unzipping mode (**Figure 5C**). The most distinguishing feature of this form of separation is the
350 high frequency in which sister acentrics aligned with their telomeres opposed (33% compared to
351 14% and 0% for sliding and unzipping separation, respectively) (**Figure 3F**). This high frequency
352 of unaligned telomeres suggests weak connections between sisters and that sister pairing is not
353 required.

354 Synthetic lethal screens have proven an effective means of identifying factors required for
355 the successful mitotic transmission of acentric chromosome fragments [12, 15]. These screens

356 have identified proteins required for poleward transmission and final incorporation of acentrics
357 into the telophase nucleus. Here we focused on identifying genes required for successful
358 separation of sister acentrics. Of the 117 candidate genes screened, we identified 23 RNAi
359 knockdowns/mutations that resulted in a significant lethality upon acentric induction (**Table 2**).
360 Live analysis secondary screening revealed knockdowns of EB1 and Map205, and the cell cycle
361 kinase Greatwall resulted in dramatic defects in acentric sister separation. Live imaging also
362 revealed reducing levels of Topoisomerase II severely disrupted sister acentric separation.

363 Given that previous studies demonstrated the chromokinesin Klp3A is required for acentric
364 poleward transport [15], it is not surprising that microtubule-associated proteins also play a key
365 role in separation of acentric sisters. Reduced levels of EB1 and Map205 greatly increase the
366 frequency of failed sister separation. EB1 is a plus-end tracking protein that associates with a
367 number of regulatory proteins and is essential for generating anti-polar forces on the
368 chromosomes [60]. EB1 knockdowns most dramatically reduce the frequency of acentric
369 separation via sliding. In addition, for those acentric sisters that did separate by sliding in EB1
370 knockdowns, separation was greatly delayed. As lateral interactions between the microtubules
371 and chromatin are likely to drive sister separation by sliding, we suspect plus-end directed EB1
372 forces may play a role in orienting the acentric in order to establish lateral interactions. Support
373 for this idea comes from the finding of a synthetic lethal interaction between I-CreI induction and
374 reductions in the levels of Nod, a non-motile chromokinesin that associates with EB1 [15, 61].
375 Map205 is a microtubule-associated protein required for targeting Polo kinase to spindle
376 microtubules [41]. Thus, it is likely that the effect of the Map205 knockdowns on acentric sister
377 separation is through disruption of Polo localization. Previous studies demonstrated that Polo
378 localizes to the DNA tether associated with the acentric and Polo knockdowns disrupted acentric
379 transmission with sister acentrics remaining on the metaphase plate [12]. As with EB1, reductions
380 in Map205 levels dramatically reduce the frequency of acentric separation by sliding suggesting
381 a disruption in lateral interactions between the acentrics and the microtubules. While much

382 evidence indicates that Polo functions at the centromere during sister separation, our studies of
383 the effects of Map205 and Polo knockdowns suggest that it is also involved in promoting
384 chromatid/spindle interactions that are independent of the centromere.

385 Reducing the levels of Topoisomerase II leads to a significant increase in failed separation
386 of sister acentrics, supporting the conclusion that once cohesin is removed sister acentrics remain
387 held together through DNA catenation. We suspect that reduced Topoisomerase II levels disrupt
388 sister separation of the acentrics more profoundly than that of intact chromosomes because the
389 latter primarily rely on kinetochore forces to resolve DNA catenations. Of the four mutants
390 analyzed through live analysis, reductions in Topoisomerase levels had the greatest effect of the
391 unzipping mode of acentric sister separation. This result is interesting given our finding that the
392 unzipping mode of acentric separation is likely the most reliant on sister pairing and consequently
393 are likely to be highly catenated.

394 Taken together, these data support a model in which multiple forces drive the separation
395 of sister acentrics. Acentrics that separate by sliding and unzipping tend to be oriented parallel
396 and perpendicular to the spindle, respectively. We view acentric sister separation by sliding as
397 largely driven by lateral microtubule interactions, while separation by unzipping as initially driven
398 by the DNA tether. Sister acentrics that separate by dissociation may be driven by a combination
399 of these forces (**Figure 8**). EB1 and Map205 may be required to establish microtubule interactions
400 with the acentric, while in the absence of a kinetochore high levels of Topoisomerase are needed
401 to resolve DNA catenations between sisters.

402 Finally, it should be noted that although these mutants resulted in a high frequency of
403 failed acentric sister separation, we did not observe an equivalent increase in micronuclei. In
404 contrast, mutants that disrupted acentric poleward transport or the final stages of incorporation
405 into daughter nuclei resulted in an accompanying increase in micronuclei [62-64]. This indicates
406 that the knockdowns in the genes identified in this study specifically disrupt acentric sister
407 separation as the subsequent transmission occurs normally to allow incorporation of the acentric

408 into the daughter nuclei. This interpretation is in accord with a model that acentrics experience
409 different forces at different stages of their separation, transmission, and incorporation into
410 daughter nuclei [64].
411

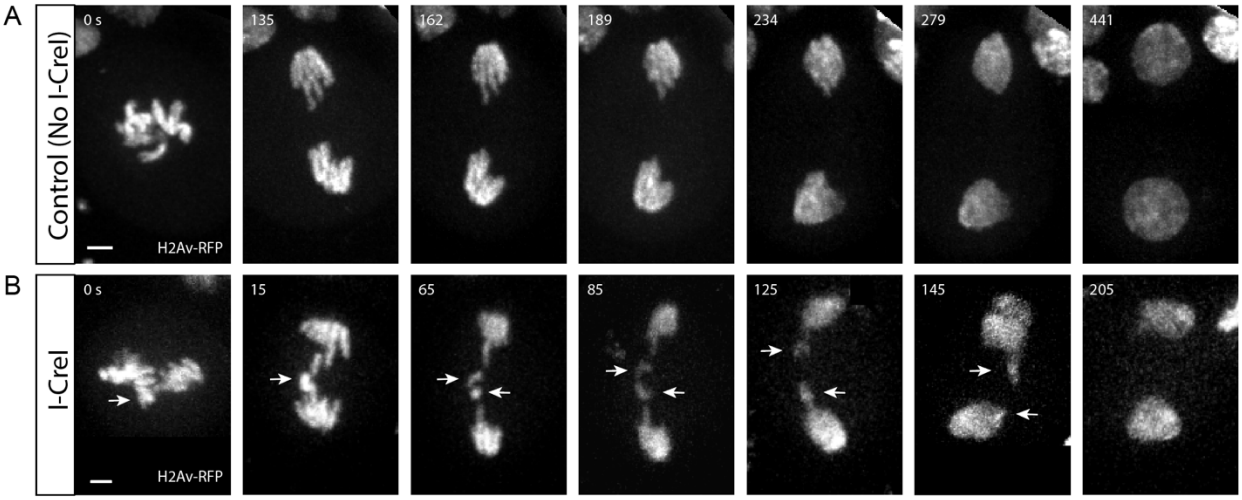

412
413 **Figure 1: Acentric sister separation is delayed relative to kinetochore-bearing**
414 **chromosomes during anaphase.** (A) Still frames of a time-lapse movie of a mitotic neuroblast
415 labeled with H2Av-RFP and not expressing I-CreI. (B) Still frames of a time-lapse movie of a
416 mitotic neuroblast with I-CreI induced acentrics. Separation of sister acentrics (arrows) is delayed.
417 Consequently, they lag on the spindle equator but eventually separate, segregate, and are
418 reincorporated into daughter nuclei. Bars, 2 μm. Time in seconds.
419

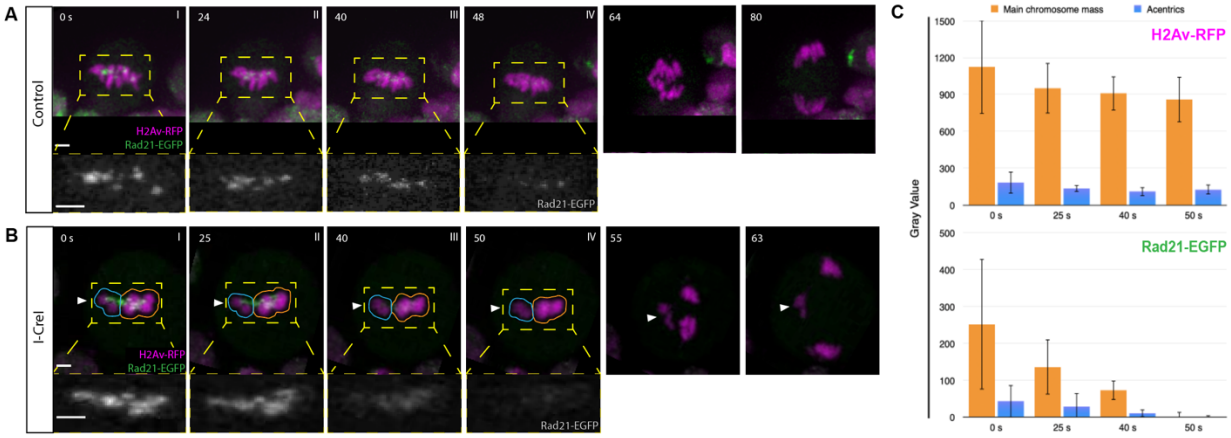

420
421 **Figure 2: Cohesin complexes are cleared off of acentric sisters upon anaphase onset.**
422 Chromosomes labeled with H2Av-RFP (magenta) and cohesin labeled with Rad21-EGFP
423 (green). (A) Stills from a time-lapse movie of a control mitotic neuroblast. (B) Still images from a
424 time-lapse movie of a mitotic neuroblast with I-CreI-induced acentrics (Movie S1). Acentrics
425 (arrowhead) lag on the spindle equator. (C) Bar graphs of a compilation of five videos of I-CreI-
426 expressing neuroblasts showing the relative fluorescence intensities in arbitrary units (AU) of
427 chromosomes (H2Av-RFP, top) cohesin (Rad21-EGFP, bottom) around acentrics (cyan outlined
428 region) and the main mass of chromosomes (yellow outlined region) at time points 50, 40, 25, 0

s, prior to anaphase onset, respectively. Bars, 2 µm. Time in seconds. Error bars represent standard deviations of fluorescence intensities at all points tested.

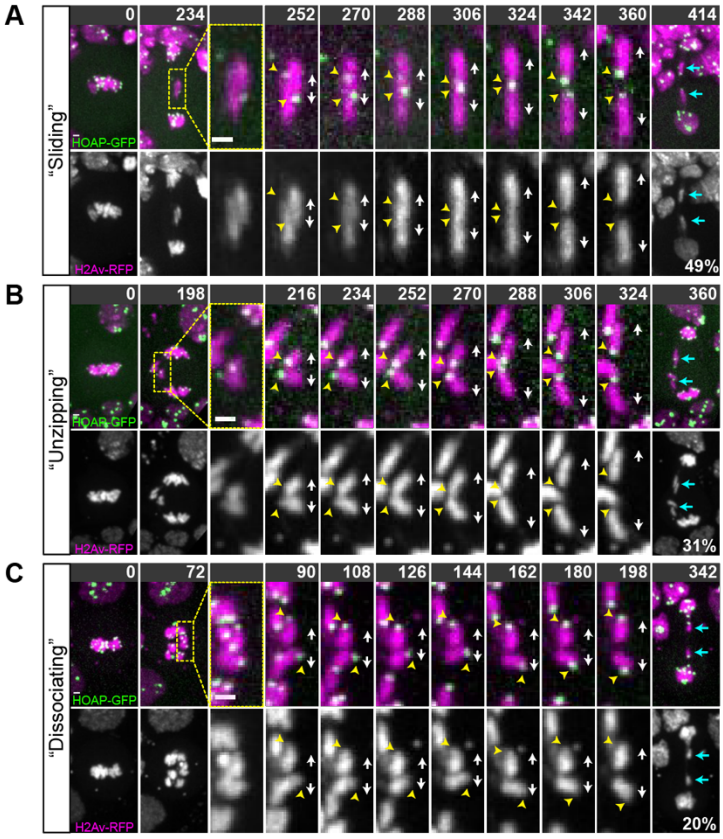

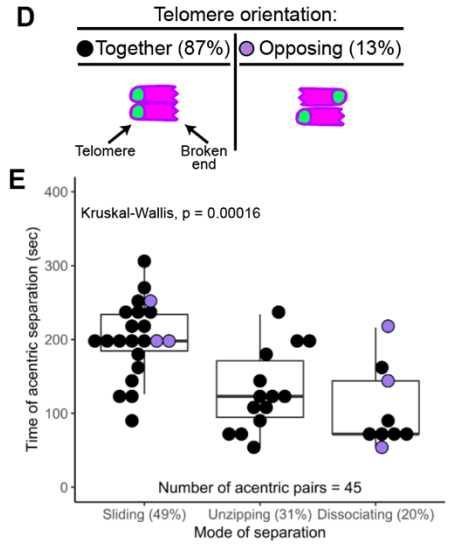

F

Mode of separation	Telomeres paired	Telomeres opposing	N
Sliding	86%	14%	22
Unzipping	100%	0%	14
Dissociating	67%	33%	9

Figure 3: Sister acentrics separate via three distinct patterns. Chromosomes labeled with H2Av-RFP (magenta) and telomeres labeled with HOAP-GFP (green). Telomeres indicated by yellow arrowheads. Direction of separation indicated by white arrows. (A) Top row: Still images of a time-lapse movie of a mitotic neuroblast with I-CreI induced acentrics showing sister acentrics (cyan arrows) lagging behind during anaphase, paired with telomeres opposing, sliding past one another, and ultimately separating. Bottom row: Black and white images of sister acentrics sliding past one another (see arrows) (Movie S2). (B) Top row: Still images of a time-lapse movie of a mitotic neuroblast with I-CreI induced acentrics showing acentrics (cyan arrows) lagging on the metaphase plate. In a process we term "unzipping", sister acentrics are aligned with telomeres paired, initiate separation at their broken ends followed by separation of telomeres. Bottom row: Black and white images of sister acentrics unzipping (see arrows). (C) Top row: Still images of a time-lapse movie of a mitotic neuroblast with I-CreI induced acentrics showing sister acentrics (cyan arrows) lagging behind during anaphase. In a process we term "dissociation", sister acentrics simultaneously separate along their entire length. Bottom row: Black and white images of sister acentrics simultaneously separating along their entire length (see arrows). (D) Frequency of acentric sisters paired with their telomeres aligned or in opposite orientations. (E) Measurements of the frequency of each mode of acentric sister separation (x-axis) and the timing of acentric sister separation after intact chromosomes separate (y-axis). Each dot represents on acentric pair. Black dots represent acentric sisters with telomeres aligned and purple dots represent acentric sisters with telomeres oriented in opposite directions. Boxes show interquartile ranges and lines show medians of the measured data. Statistical significance was determined by

a Kruskal-Wallis test. (F) Chart showing the distribution of telomere orientations within each mode of acentric sister separation. Acentrics that separate by unzipping are always oriented with their telomeres paired.

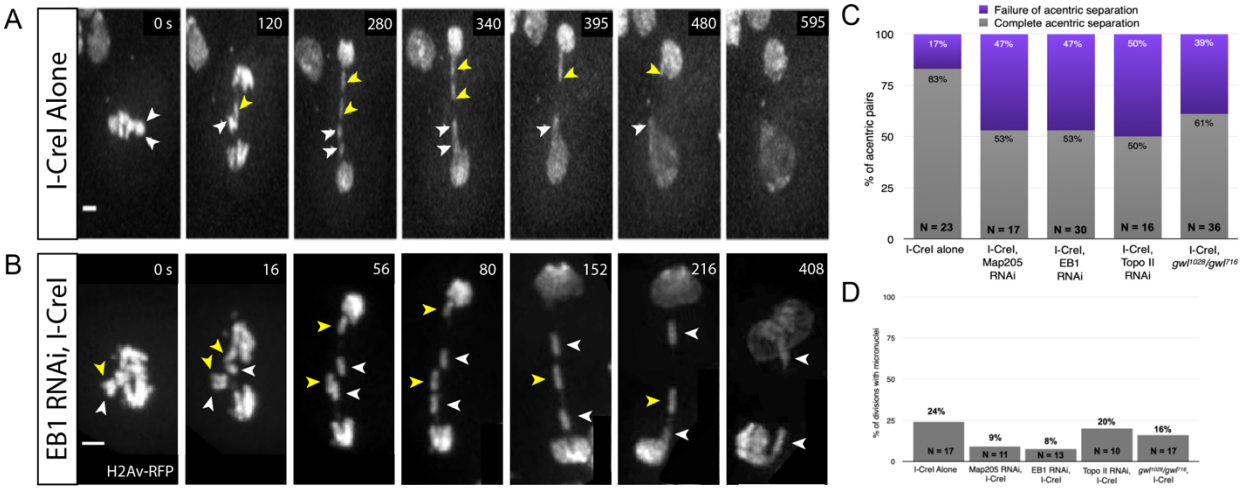

Figure 4: EB1 RNAi knockdowns specifically disrupt acentric sister separation. (A) Still frames of a time-lapse movie of a mitotic neuroblast with I-CreI induced acentrics. Paired sister acentrics (white and yellow arrowheads) lag behind at the spindle equator but eventually separate, segregate, and are reincorporated into daughter nuclei. (B) Still frames of a time-lapse movie of a mitotic neuroblast with I-CreI induced acentrics and expressing EB1 RNAi. Separation of paired sister acentrics (white and yellow arrowheads) fails, resulting in sisters segregating to and incorporating into the same daughter nucleus. Bars, 2 µm. Time in seconds. (Video 3) (C) Percentages of neuroblast divisions in which acentric sisters failed to completely separate from one another. (D) Percentages of neuroblast divisions in which acentrics failed to incorporate into daughter nuclei and formed one or more micronuclei.

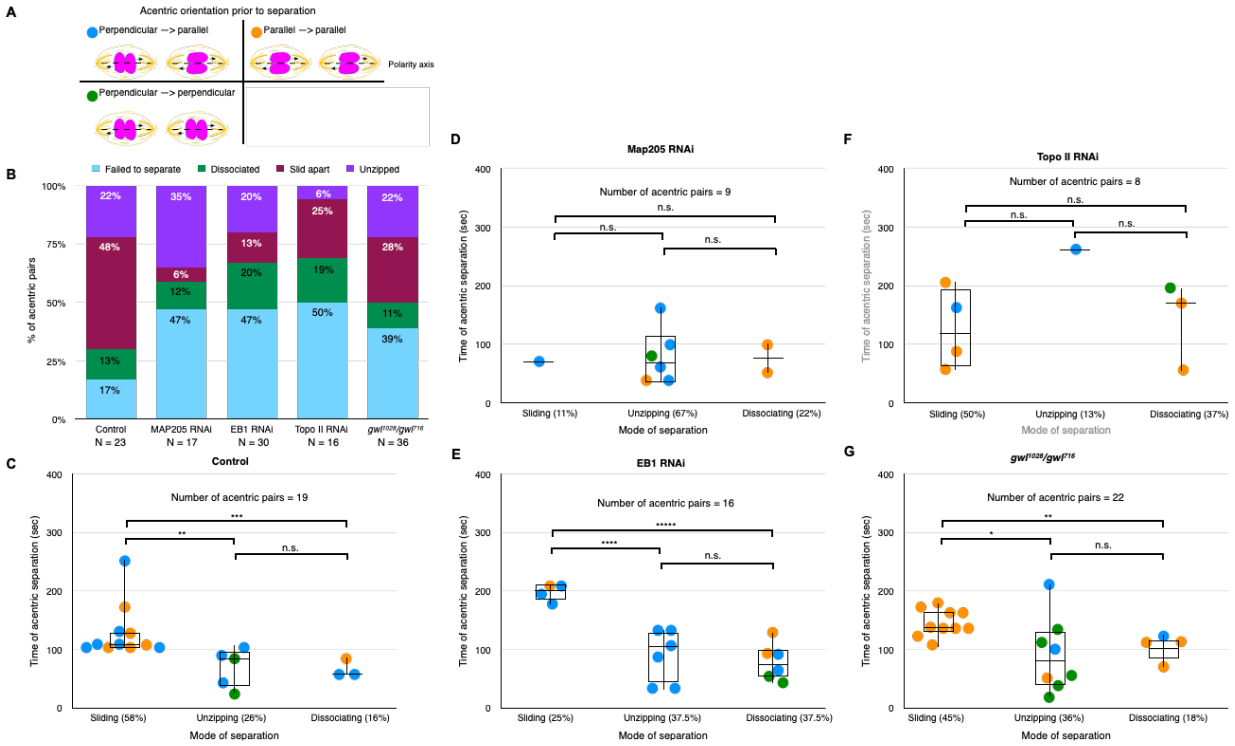

Figure 5: Knockdowns of EB1 and Map205 preferentially disrupt the sliding mode of acentric separation. (A) Model of different acentric orientations prior to separation. Polarity axis indicated by the dotted line. (B) Bar graph showing the percentage of acentric pairs that separate via dissociation, sliding, or unzipping and the percentage of those that fail to separate. (C-G) Measurements of the frequency of each mode of acentric sister separation (x-axis) and the timing of acentric sister separation after the separation of intact chromosomes (y-axis). Each dot represents one acentric pair. Blue dots represent acentric pairs that were oriented perpendicular then parallel to the polarity axis prior to separation. Orange dots represent acentric pairs that were oriented parallel to the polarity axis prior to separation. Green dots represent acentric pairs that were oriented perpendicular to the polarity axis prior to separation. Boxes show interquartile ranges and lines show medians of the measured data. Asterisks indicate statistical significance (*P = 0.04, **P = 0.02, ***P = 0.005, ****P = 0.0007, *****P = 0.00004) determined by a two-tailed T-test. Non-significant values had a P-value greater than 0.05.

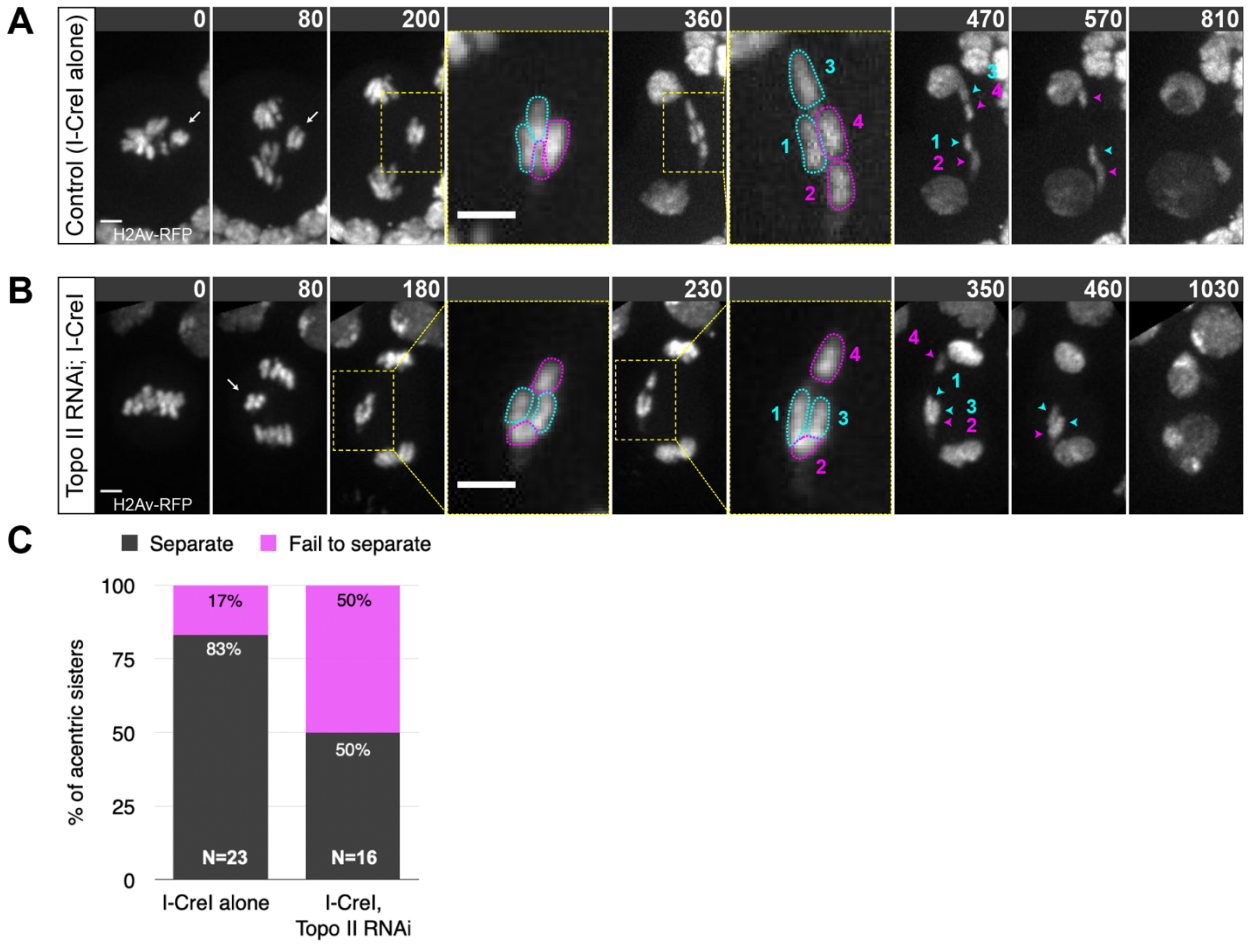

Figure 6: Acentrics appear to be held together by DNA catenations. (A) Still images of a time-lapse movie of a control neuroblast with I-CreI induced acentrics showing sister acentrics associated in early anaphase (white arrows), lagging behind and ultimately separating and segregating to opposite poles (cyan and magenta arrowheads). (B) Still images of a time-lapse movie of a neuroblast with partial knockdown of Topoisomerase II using RNAi and I-CreI induced acentrics. Acentrics associate and lag behind in early anaphase (white arrow), then fail to completely separate and segregate unequally (cyan and magenta arrowheads). Bars, 2 μm. Time in seconds. (Movie S4) (C) Bar graph showing the quantification of acentric behavior in control and Topo II RNAi neuroblasts with the failure of acentric sister separation in magenta and the successful, even separation of acentric sisters in gray.

512

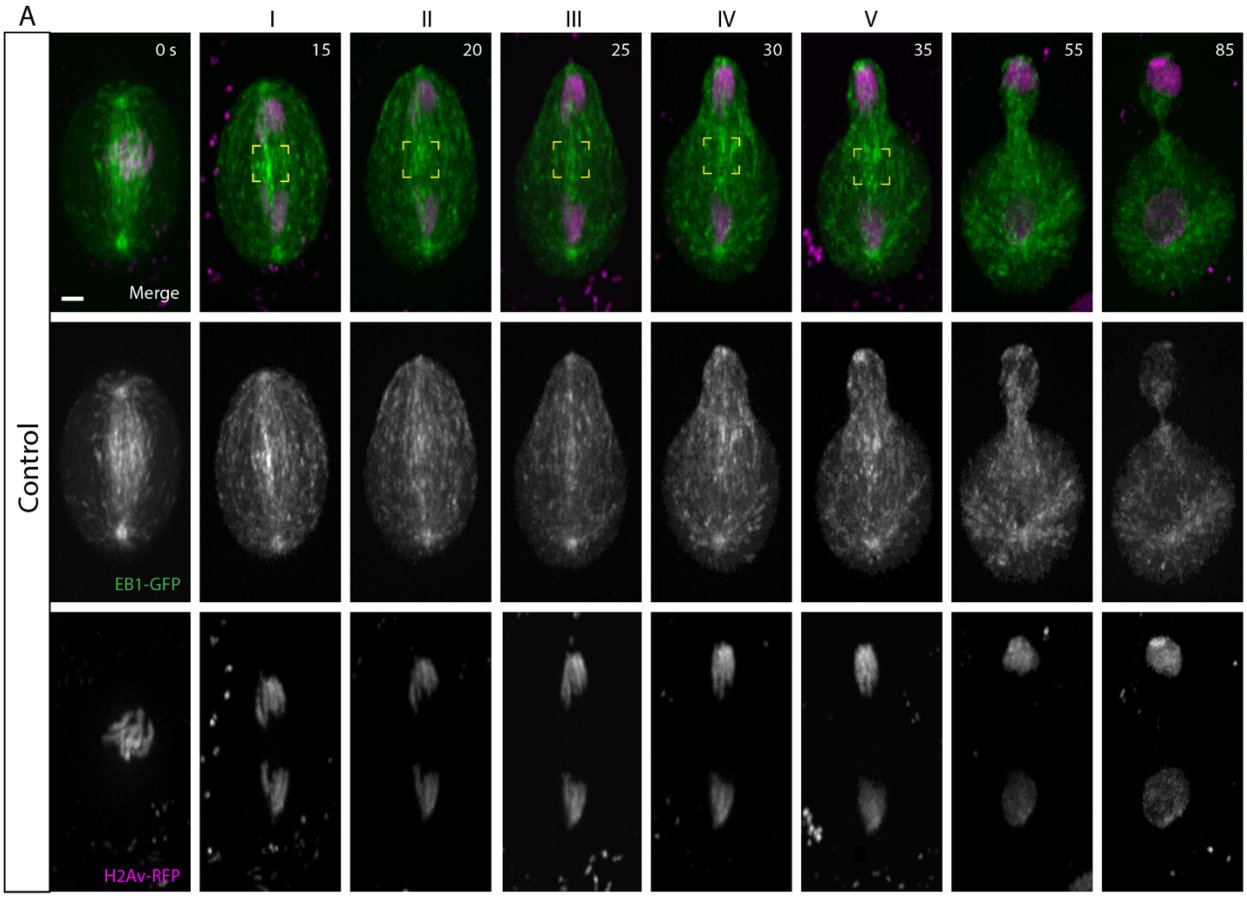
A
I
II
III
IV
V
0 s
15
20
25
30
35
55
85
Merge
Control
EB1-GFP
H2Av-RFP

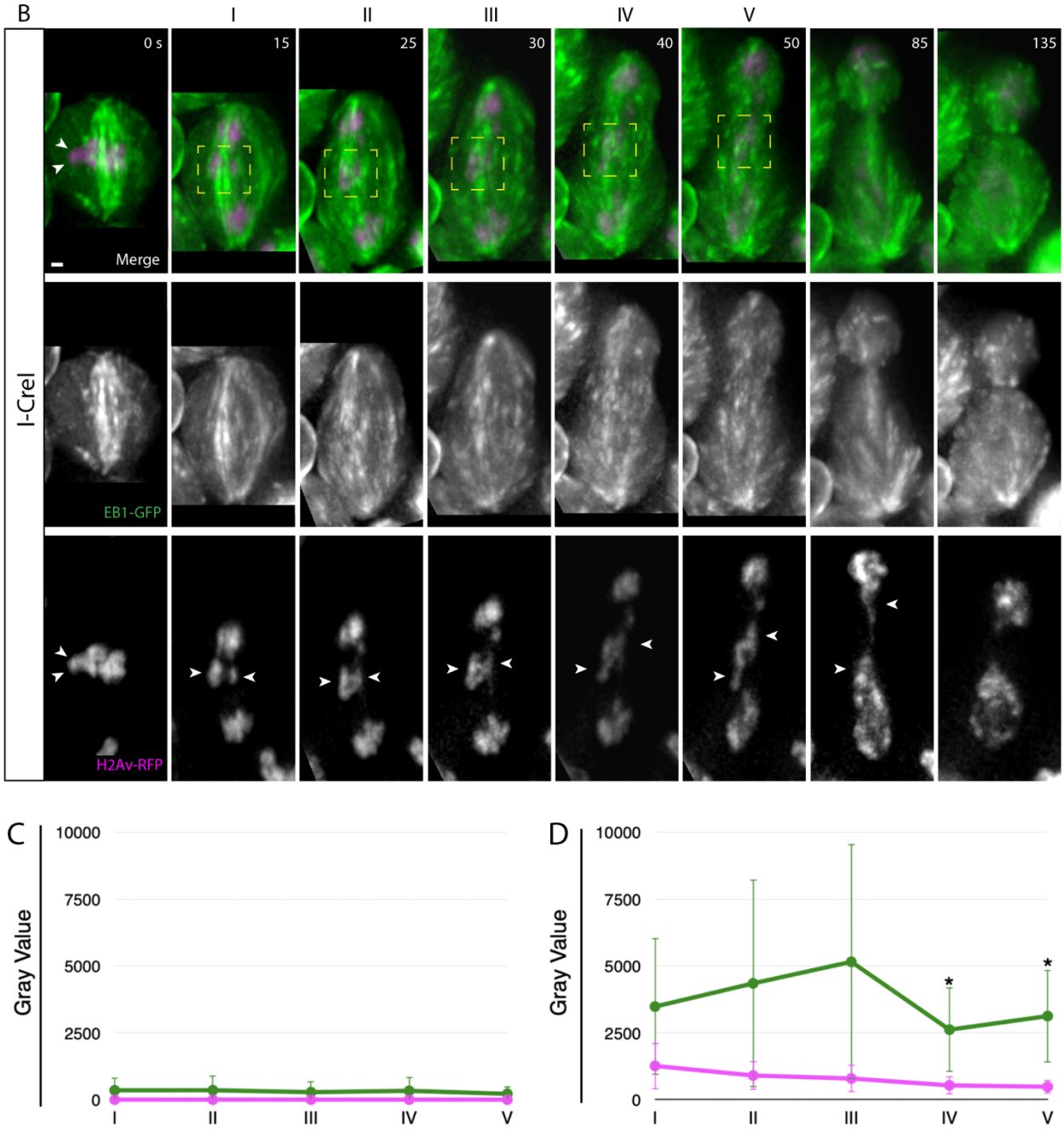

Figure 7: Acentrics travel poleward in late anaphase while associated with EB1. EB1 is in green and chromosomes are in magenta. (A) Still images from a time-lapse movie of a control neuroblast from metaphase (0 s) through telophase (85 s). (B) Still images from a time-lapse movie of a mitotic neuroblast with I-CreI induced acentrics from metaphase (0 s) through telophase (135 s) (Movie S5). The intact chromosomes and acentrics initiate sister separation at the 15 s and 40 s timepoints, respectively. Sister acentrics (white arrowheads) separate and move toward opposite cell poles while associated with EB1. (C) Line graph from a compilation of five control videos showing the corrected fluorescence intensities in arbitrary units (AU) of EB1 (green) and chromosomes (magenta). Corrected fluorescence intensities were calculated within the yellow boxes at the time points 15, 20, 25, 30, 35 seconds after anaphase onset. (D) Line graph

from a compilation of five videos of I-CreI-expressing neuroblasts showing the corrected fluorescence intensities in arbitrary units (AU) of EB1 (green) and chromosomes (magenta). Corrected fluorescence intensities were calculated within the yellow boxes at the time points 15, 25, 30, 40, 50 seconds after anaphase. Bars, 2 μm. Time in seconds. Error bars represent SDs of the fluorescent intensities at all points tested.

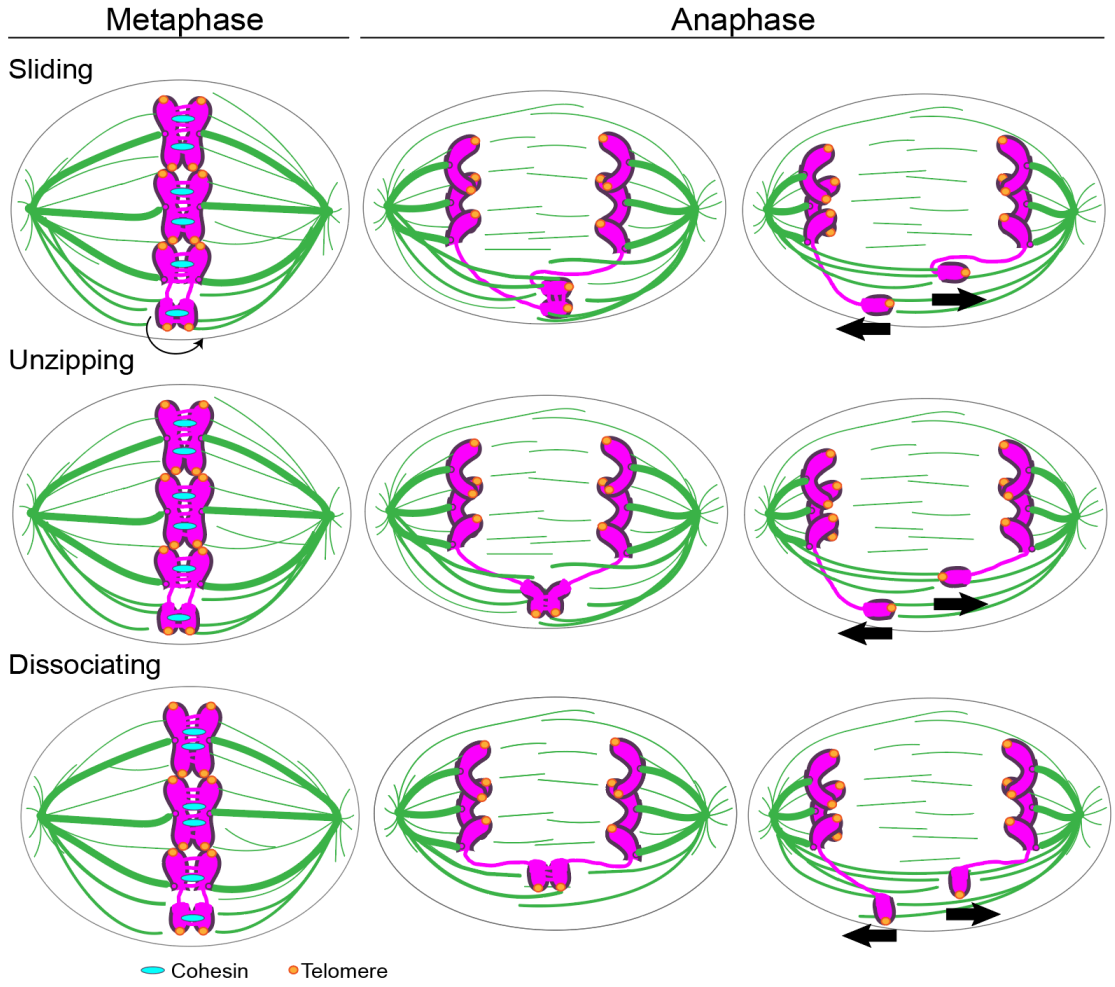

Figure 8: Schematic showing distinct modes of acentric separation. At some point during the metaphase-to-anaphase transition, acentrics that separate by sliding orient parallel to the spindle and slide past one another. This is likely driven by lateral associations between the microtubules and acentrics. The unzipping mode occurs when separation initiates at the broken end followed by separation of sister telomeres. It may be that the initial separation is driven by the DNA tether connecting the centric and acentric fragments. Simultaneous separation across the entire length of the acentric is referred to as dissociation. It may be that the DNA tether and acentric-microtubule interactions contribute equally for sister acentrics that separate by dissociation. (Chromosomes in magenta, microtubules in green, cohesin in cyan, telomeres in orange).

549 **Table 1: Average timing of acentric separation.**
550

	Avg ± SD (seconds)	N (acentric pairs)
Control	100 ± 48	19
MAP205 RNAi	78 ± 38	9
EB1 RNAi	113 ± 59	16
Topo II RNAi	150 ± 76	8
***gwl*^{1028}/*gwl*^{716}**	117 ± 49	22

551
552
553
554 **Table 2: Top hits from synthetic lethality screen.**
555

	Gene RNAi	Survival rate with RNAi and I-CreI induced / Only RNAi induced	Rate of larvae-to-adult survival of RNAi with I-CreI induction % ± SD (N)	Rate of larvae-to-adult survival of RNAi without I-CreI induction % ± SD (N)	Gene function
	Wildtype (Control)		80 ± 21 (194)	91 ± 7 (194)	—
Chromatin-associated:	*hyx* (2)	10%	8 (25)	88 (25)	Transcription factor
	cap-D2	12%	6 (17)	50 (12)	Condensin
	chd1	30%	10 ± 17 (69)	33 ± 6 (99)	ATP-dependent chromatin remodeling
	sin3A	33%	8 (25)	24 (25)	Histone deacetylase, transcription regulator
	chrac-14 (2)	48%	48 (25)	100 (25)	Nucleosome mobilization, chromatin assembly
	chd1 (2)	50%	48 (25)	95 (23)	ATP-dependent chromatin remodeling
	spt4	55%	24 (25)	44 (25)	Transcription elongation factor
	sir2	60%	64 (25)	94 (16)	Histone deacetylase, heterochromatin gene silencing
	hp1e	65%	65 (20)	100 (25)	Heterochromatin protein 1 (chromosome segregation)
Microtubule-associated:	*msps*	27%	18 ± 17 (56)	67 ± 24 (30)	Mitotic spindle, microtubule nucleation
	asp (2)	46%	44 (25)	96 (25)	Astral microtubule organization, spindle orientation
	EB1	47%	44 ± 25 (86)	94 ± 9 (38)	Microtubule plus-end binding, chromosome segregation
	Klp68D	51%	29 (24)	57 (21)	Kinesin motor protein, microtubule-based transport
	asp	52%	52 (25)	100 (15)	Astral microtubule organization, spindle orientation
	map205	65%	54 ± 18 (141)	83 ± 13 (91)	Binds/stabilizes microtubules
DNA repair/ checkpoint:	*spnA*	2%	2 ± 4 (57)	82 ± 18 (99)	Rad51 double-strand break repair
	mus309	11%	10 ± 1 (42)	95 (22)	Double-strand break repair
	ku80	29%	28 (25)	96 (25)	Non-homologous end joining double-strand break repair
	tefu	43%	43 (30)	100 (25)	DNA damage checkpoint
	cp190	48%	12 (17)	25 (12)	Chromatin silencing, DNA damage response
Cell cycle kinase:	*bubR1*	3%	1 ± 2 (168)	31 ± 23 (69)	Mitotic exit and spindle checkpoint kinase
	gwl (2)	8%	2 ± 2 (112)	26 ± 10 (99)	Negative PP2A regulator and mitotic exit kinase
	ald	59%	52 (25)	88 (25)	Altered disjunction, chromosome separation kinase

556
557
558

559 **Table 3: Average rates of acentric segregation.**
560

	Avg velocity ± SD (nm/s)	N (individual acentrics)
Control	10 ± 4	26
MAP205 RNAi	12 ± 5	30
EB1 RNAi	10 ± 4	27
Topo II RNAi	12 ± 3	26
***gwl*^{1028}/*gwl*^{716}**	8 ± 4	32

561
562
563
564 **Table 4: Distribution of modes of acentric separation.**
565

	Failed to separate	Disassociated	Slid Apart	Unzipped	N (acentric pairs)
Control	17%	13%	48%	22%	23
MAP205 RNAi	47%	12%	6%	35%	17
EB1 RNAi	47%	20%	13%	20%	30
Topo II RNAi	50%	19%	25%	6%	16
***gwl*^{1028}/*gwl*^{716}**	39%	11%	28%	22%	36

566
567
568
569
570
571
572
573
574
575
576
577
578
579
580
581
582
583
584
585
586
587
588
589
590

591 **MATERIALS AND METHODS**

592 Fly Stocks

593 All stocks were raised on standard *Drosophila* media at room temperature (20-22°C). For
594 generating acentrics, a transgenic fly line bearing the I-CreI endonuclease under heat-shock 70
595 promoter were kindly provided by Kent Golic at The University of Utah. For synthetic lethality
596 screen, the ubiquitous Gal4 driver under the control of an actin enhancer (Act5) was used (#25708
597 from Bloomington). Dominant negative allele of ISWI was kindly provided by John Tamkun at UC
598 Santa Cruz. Greatwall hypomorphs (*gwl*$^{1080,\ 716,\ 180,\ and\ 2790}$) were kindly provided by Michael
599 Goldberg at Cornell University. The line with *rad21-EGFP* transgene were kindly provided by
600 Stefan Heidmann at University of Bayreuth.

601

602 Synthetic Lethality Screen

603 Third instar progeny with genotype Act5-Gal4/+; I-CreI, Sb/UAS-RNAi were collected from
604 parental genotypes Act5-Gal4/CyO-GFP; I-CreI, Sb/TM6B and were heat shocked for 1.5 hours
605 at 37°C (unless otherwise indicated). After heat shock, the vials were set-aside at room
606 temperature for 10-15 days until adult flies emerged. Synthetic lethality was calculated as the %
607 of larvae that develop into adulthood. Control progeny with genotype Act5-Gal4/+; Sb/UAS-RNAi
608 from parents with the genotype Act5-Gal4/CyO-GFP; Sb/TM6B and UAS-RNAi were heat-
609 shocked for 1.5 hours at 37°C.

610

611 Live analysis of acentric behavior in *Drosophila* third instar neuroblasts

612 Acentric chromosome fragments were induced by I-CreI expression (under heat shock 70
613 promoter) in 3rd instar larvae by a 1-hour 37°C heat shock followed by a 1-hour recovery period
614 at room temperature. The larval brains from third instar larvae were dissected in PBS and then
615 transferred to a slide with 20 µl of PBS. A coverslip was dropped on PBS solution with brain and
616 the excess PBS solution was wicked out from edge of coverslip to induce squashing of brain

617 between slide and coverslip. For live analysis, the edge of coverslip was sealed with halocarbon
618 and was imaged as described below. Neuroblast divisions in all images were from female 3rd
619 instar larvae.
620
621 Microscopy and image acquisition
622 *Wide-field microscopy*
623 Time-lapse imaging for Figure 4C, 4D, 5, and 5C was acquired with a Leica DM16000B wide-field
624 inverted microscope with a Hamamatsu electron-multiplying charge coupled device camera
625 (ORCA 9100-02) with a binning of 1 and a 1.4 NA 100x Plan-Apochromat objective. Signal from
626 RFP and GFP fluorophores was collected at 585 nm and 508 nm, respectively. Time-lapse videos
627 were done every 20 seconds. Imaging was performed at room temperature. Images were
628 acquired using the Leica Application Suite Advanced Fluorescence Software. 3D deconvolution
629 was performed using AutoQuant X2.2.0.
630
631 *Spinning-disk microscopy*
632 Images in Figures 1, 2, 3, 4A, 4B, 6A, 6B, and 7 were acquired with an inverted Nikon Eclipse
633 TE2000-E spinning disk (CSLI-X1) confocal microscope equipped with a Hamamatsu electron-
634 multiplying charge coupled device camera (ImageEM X2) with a 100X 1.4 NA oil-immersion
635 objective. Imaging was performed at room temperature. Images were acquired with
636 MicroManager 1.4 software. Time-lapse fluorescent images of neuroblasts divisions were done
637 with 120 and 100 ms exposures for GFP and RFP, respectively, with 0.5 μm Z-steps. Time-lapse
638 videos with both GFP and RFP were done every 5 to 18 seconds and time-lapse movies with
639 RFP alone were done every 5 to 10 seconds. Figures were assembled in Adobe Illustrator.
640 Selected stills (both experimental and control) were processed with ImageJ
641 (http://rsb.info.nih.gov/ij/).
642

643
644
645 Measurements
646
647 In Figures 2B and 2C, relative fluorescence intensities of chromosomes (H2Av-RFP) and cohesin
648 (Rad21-EGFP) were done by calculating the corrected total cell fluorescence (CTCF) using
649 ImageJ of the region outlined around acentrics and the main mass of chromosomes. CTCF =
650 integrated density – (area of selected region in cell * mean fluorescence of background readings).
651 In Figure 7, relative fluorescence intensities of acentrics (H2Av-RFP) and EB1 (EB1-EGFP) were
652 done by calculating the CTCF using integrated density, area, and mean fluorescence of the
653 background acquired from ImageJ of the region outlined around acentrics in I-CreI expressing
654 neuroblasts and the region outlined around the spindle midzone in control neuroblasts. The area
655 of the boxes outlining acentrics and spindle midzones were kept consistent for each cell. In Table
656 3, velocities of acentric segregation were calculated as distance (micrometers)/time (seconds).
657 For statistical analyses, unpaired two-sided t-tests and two-sided Mann-Whitney-Wilcoxon tests
658 were used. Unpaired two-sided t-tests were performed in Prism Version 8 (GraphPad Software).
659 Two-sided Mann-Whitney-Wilcoxon tests and Kruskal-Wallis tests were performed in R (R Core
660 Team).
661
662 **ACKNOWLEDGEMENTS**
663
664 We would like to thank Dr. Susan Strome, Dr. William Saxton, and Dr. John Tamkun for use of
665 their equipment and providing reagents. We thank Dr. Benjamin Abrams for his advice and
666 technical expertise regarding microscopy experiments. We thank Dr. Kent Golic for providing us
667 with the transgenic fly line bearing the I-CreI endonuclease. We thank Dr. Michael Goldberg for
668 providing us with Greatwall hypomorph flies. We thank Dr. Stefan Heidmann for providing us with
669 the transgenic fly line bearing *rad21-EGFP*. We thank H. Vicars' service dog Teddy Bear for his
670 guidance and support.
671

Funding for these studies was provided by National Institutes of Health grant NIH1RO1GM120321 awarded to W. Sullivan.

The authors declare no competing financial interests.

REFERENCES

1. Ermolaeva MA, Schumacher B. Systemic DNA damage responses: Organismal adaptations to genome instability. Trends Genet. 2014;30(3):95–102. pmid:24439457; PubMed Central PMCID: PMC4248340

2. Mikhailov A, Cole RW, Rieder CL. DNA Damage during Mitosis in Human Cells Delays the Metaphase/Anaphase Transition via the Spindle-Assembly Checkpoint. Current Biology. 2002;12(21):1797–806. pmid:12419179

3. Royou A, Macias H, Sullivan W. The Drosophila Grp/Chk1 DNA Damage Checkpoint Controls Entry into Anaphase. Current Biology. 2005;15(4):334–9. pmid:15723794

4. Coutelier H, Xu Z. Adaptation in replicative senescence: a risky business. Curr Genet. 2019;65(3):711–6. pmid:30637477

5. Kanda T, Wahl GM. The dynamics of acentric chromosomes in cancer cells revealed by GFP-based chromosome labeling strategies. J Cell Biochem Suppl. 2000; Suppl 35:107–14. pmid:11389539

6. LaFountain JR, Oldenbourg R, Cole RW, Rieder CL. Microtubule Flux Mediates Poleward Motion of Acentric Chromosome Fragments during Meiosis in Insect Spermatocytes. Mol Biol Cell. 2001;12(12):4054–65. pmid:11739800; PubMed Central PMCID: PMC60775

7. Fenech M, Kirsch-Volders M, Natarajan AT, Surralles J, Crott JW, Parry J, et al. Molecular mechanisms of micronucleus, nucleoplasmic bridge and nuclear bud formation in mammalian and human cells. Mutagenesis. 2011;26(1):125–32. pmid:21164193

8. Bajer A. Cine-micrographic studies on chromosome movements in β-irradiated cell. Chromosoma. 1958;9:319-331. pmid:13608834

9. Liang H, Wright WH, Cheng S, He W, Berns MW. Micromanipulation of chromosomes in PTK2 cells using laser microsurgery (optical scalpel) in combination with laser-induced optical force (optical tweezers). Experimental cell research. 1993;204(1):110–20. pmid:8416789

10. Khodjakov A, Cole RW, Bajer AS, Rieder CL. The force for poleward chromosome motion in Haemanthus cells acts along the length of the chromosome during metaphase but only at the kinetochore during anaphase. J Cell Biol. 1996;132(6):1093–104. pmid:8601587; PubMed Central PMCID: PMC2120764

11. Kanda T, Sullivan KF, Wahl GM. Histone–GFP fusion protein enables sensitive analysis of chromosome dynamics in living mammalian cells. Current Biology. 1998;8(7):377–85. pmid:9545195

12. Royou A, Gagou ME, Karess R, Sullivan W. BubR1- and Polo-Coated DNA Tethers Facilitate Poleward Segregation of Acentric Chromatids. Cell. 2010;140(2):235–45. pmid:20141837; PubMed Central PMCID: PMC2969851

13. Bretscher HS, Fox DT. Proliferation of Double Strand Break Resistant Polyploid Cells Requires Drosophila FANCD2. Dev Cell. 2016;37(5):444–57. pmid:27270041; PubMed Central PMCID: PMC4901310

14. Platero JS, Ahmad K, Henikoff S. A Distal Heterochromatic Block Displays Centromeric Activity When Detached from a Natural Centromere. Molecular Cell. 1999;4(6):995–1004. pmid:10635324

15. Karg T, Elting MW, Vicars H, Dumont S, Sullivan W. The chromokinesin Klp3a and microtubules facilitate acentric chromosome segregation. J Cell Biol. 2017;216(6):1597–608. pmid:28500183; PubMed Central PMCID: PMC5461011

16. Kanda T, Otter M, Wahl GM. Mitotic segregation of viral and cellular acentric extrachromosomal molecules by chromosome tethering. J Cell Sci. 2001; 114:49-58. pmid:11112689

17. Ishii K, Ogiyama Y, Chikashige Y, Soejima S, Masuda F, Kakuma T, et al. Heterochromatin Integrity Affects Chromosome Reorganization After Centromere Dysfunction. Science. 2008;321(5892):1088–91. pmid:18719285

18. Ohno Y, Ogiyama Y, Kubota Y, Kubo T, Ishii K. Acentric chromosome ends are prone to fusion with functional chromosome ends through a homology-directed rearrangement. Nucleic Acids Res. 2016;44(1):232–44. pmid:26433224; PubMed Central PMCID: PMC4705696

19. Rong YS, Titen SW, Xie HB, Golic MM, Bastiani M, Bandyopadhyay P, et al. Targeted mutagenesis by homologous recombination in D. melanogaster. Genes Dev. 2002;16(12):1568–81. pmid:12080094; PubMed Central PMCID: PMC186348

20. Maggert KA, Golic KG. Highly Efficient Sex Chromosome Interchanges Produced By I-CreI Expression in Drosophila. Genetics. 2005;171(3):1103–14. pmid:16020774; PubMed Central PMCID: PMC1456814

21. Paredes S, Maggert KA. Ribosomal DNA contributes to global chromatin regulation. Proc Natl Acad Sci U S A. 2009;106(42):17829–34. pmid:19822756; PubMed Central PMCID: PMC2764911

22. Golic MM, Golic KG. A simple and rapid method for constructing ring-X chromosomes in Drosophila melanogaster. Chromosoma. 2011;120(2):159–64. pmid:21085980; PubMed Central PMCID: PMC4454366

23. Guacci V, Koshland D, Strunnikov A. A Direct Link between Sister Chromatid Cohesion and Chromosome Condensation Revealed through the Analysis of MCD1 in S. cerevisiae. Cell. 1997;91(1):47–57. pmid:9335334; PubMed Central PMCID: PMC2670185

24. Michaelis C, Ciosk R, Nasmyth K. Cohesins: Chromosomal Proteins that Prevent Premature Separation of Sister Chromatids. Cell. 1997;91(1):35–45. pmid:9335333

25. Uhlmann F, Lottspeich F, Nasmyth K. Sister-chromatid separation at anaphase onset is promoted by cleavage of the cohesin subunit Scc1. Nature. 1999;400(6739):37–42. pmid:10403247

26. Uhlmann F, Wernic D, Poupart M-A, Koonin EV, Nasmyth K. Cleavage of Cohesin by the CD Clan Protease Separin Triggers Anaphase in Yeast. Cell. 2000;103(3):375–86. pmid:11081625

27. Oliveira RA, Hamilton RS, Pauli A, Davis I, Nasmyth K. Cohesin cleavage and Cdk inhibition trigger formation of daughter nuclei. Nat Cell Biol. 2010;12(2):185–92. pmid:20081838; PubMed Central PMCID: PMC3284228

28. Gutiérrez-Caballero C, Cebollero LR, Pendás AM. Shugoshins: from protectors of cohesion to versatile adaptors at the centromere. Trends in Genetics. 2012;28(7):351–60. pmid:22542109

29. Asbury CL. Anaphase A: Disassembling Microtubules Move Chromosomes toward Spindle Poles. Biology. 2017;6(1):15. pmid:28218660; PubMed Central PMCID: PMC5372008

30. Oliveira RA, Kotadia S, Tavares A, Mirkovic M, Bowlin K, Eichinger CS, et al. Centromere-Independent Accumulation of Cohesin at Ectopic Heterochromatin Sites Induces Chromosome Stretching during Anaphase. PLoS Biol. 2014;12(10):e1001962. pmid:25290697; PubMed Central PMCID: PMC4188515

31. Urban E, Nagarkar-Jaiswal S, Lehner CF, Heidmann SK. The Cohesin Subunit Rad21 Is Required for Synaptonemal Complex Maintenance, but Not Sister Chromatid Cohesion, during Drosophila Female Meiosis. PLoS Genet. 2014;10(8):e1004540. pmid:25101996; PubMed Central PMCID: PMC4125089

32. Cenci G, Siriaco G, Raffa GD, Kellum R, Gatti M. The Drosophila HOAP protein is required for telomere capping. Nat Cell Biol. 2003;5(1):82–4. pmid:12510197

33. Staeva-Vieira E, Yoo S, Lehmann R. An essential role of DmRad51/SpnA in DNA repair and meiotic checkpoint control. EMBO J. 2003;22(21):5863–74. pmid:14592983; PubMed Central PMCID: PMC275421

34. McVey M, Andersen SL, Broze Y, Sekelsky J. Multiple Functions of Drosophila BLM Helicase in Maintenance of Genome Stability. Genetics. 2007;176(4):1979–92. pmid:17507683; PubMed Central PMCID: PMC1950607

35. Melnikova L, Biessmann H, Georgiev P. The Ku Protein Complex Is Involved in Length Regulation of Drosophila Telomeres. Genetics. 2005;170(1):221–35. pmid:15781709; PubMed Central PMCID: PMC1449706

36. Oikemus SR, McGinnis N, Queiroz-Machado J, Tukachinsky H, Takada S, Sunkel CE, et al. Drosophila atm/telomere fusion is required for telomeric localization of HP1 and telomere position effect. Genes Dev. 2004;18(15):1850–61. pmid:15256487; PubMed Central PMCID: PMC517405

37. Moon W, Hazelrigg T. The Drosophila Microtubule-Associated Protein Mini Spindles Is Required for Cytoplasmic Microtubules in Oogenesis. Current Biology. 2004;14(21):1957–61. pmid:15530399

38. Saunders RDC, Avides M do C, Howard T, Gonzalez C, Glover DM. The Drosophila Gene abnormal spindle Encodes a Novel Microtubule-associated Protein That Associates with the Polar Regions of the Mitotic Spindle. J Cell Biol. 1997;137(4):881–90. pmid:9151690; PubMed Central PMCID: PMC2139842

39. Rogers SL, Rogers GC, Sharp DJ, Vale RD. Drosophila EB1 is important for proper assembly, dynamics, and positioning of the mitotic spindle. J Cell Biol. 2002;158(5):873–84. pmid:12213835; PubMed Central PMCID: PMC2173155

40. Pesavento PA, Stewart RJ, Goldstein LS. Characterization of the KLP68D kinesin-like protein in Drosophila: possible roles in axonal transport. The Journal of Cell Biology. 1994;127(4):1041–8. pmid:7525600; pmid:7525600; PubMed Central PMCID: PMC2200055

41. Archambault V, D'Avino PP, Deery MJ, Lilley KS, Glover DM. Sequestration of Polo kinase to microtubules by phosphopriming-independent binding to Map205 is relieved by phosphorylation at a CDK site in mitosis. Genes Dev. 2008;22(19):2707–20. pmid:18832073; PubMed Central PMCID: PMC2559908

42. Savvidou E, Cobbe N, Steffensen S, Cotterill S, Heck MMS. Drosophila CAP-D2 is required for condensin complex stability and resolution of sister chromatids. Journal of Cell Science. 2005;118(11):2529–43. pmid:15923665

43. Stokes DG, Tartof KD, Perry RP. CHD1 is concentrated in interbands and puffed regions of Drosophila polytene chromosomes. Proc Natl Acad Sci USA. 1996;93(14):7137–42. pmid:8692958; PubMed Central PMCID: PMC38949

44. Feller C, Forné I, Imhof A, Becker PB. Global and Specific Responses of the Histone Acetylome to Systematic Perturbation. Molecular Cell. 2015;57(3):559–71. pmid:25578876

45. Corona DFV, Eberharter A, Budde A, Deuring R, Ferrari S, Varga-Weisz P, et al. Two histone fold proteins, CHRAC-14 and CHRAC-16, are developmentally regulated subunits of chromatin accessibility complex (CHRAC). EMBO J. 2000;19(12):3049–59. pmid:10856248; PubMed Central PMCID: PMC203371

46. Eissenberg JC, Elgin SCR. HP1a: A Structural Chromosomal Protein Regulating Transcription. Trends Genet. 2014;30(3):103–10. pmid:24555990; PubMed Central PMCID: PMC3991861

47. Yu J, Fleming SL, Williams B, Williams EV, Li Z, Somma P, et al. Greatwall kinase: a nuclear protein required for proper chromosome condensation and mitotic progression in Drosophila. J Cell Biol. 2004;164:487-492. pmid:14970188; PubMed Central PMCID: PMC2171981

48. O'Tousa J. Meiotic chromosome behavior influenced by mutation-altered disjunction in Drosophila melanogaster females. Genetics. 1982;102:503-524. pmid:6816677; PubMed Central PMCID: PMC1201954

49. Schuh M, Lehner CF, Heidmann S. Incorporation of Drosophila CID/CENP-A and CENP-C into centromeres during early embryonic anaphase. Curr Biol. 2007;17(3):237-243. pmid:17222555

50. Porter ACG, Farr CJ. Topoisomerase II: untangling its contribution at the centromere. Chromosome Res. 2004;12(6):569–83. pmid:15289664

51. Voets E, Wolthuis RMF. MASTL is the human orthologue of Greatwall kinase that facilitates mitotic entry, anaphase and cytokinesis. Cell Cycle. 2010;9(17):3591-601. pmid:20818157

52. Vukušić K, Buđa R, Tolić IM. Force-generating mechanisms of anaphase in human cells. J Cell Sci. 2019;132(18):jcs231985. pmid:31527150

53. Toyoda Y, Yanagida M. Coordinated Requirements of Human Topo II and Cohesin for Metaphase Centromere Alignment under Mad2-dependent Spindle Checkpoint Surveillance. Mol Biol Cell. 2006;17(5):2287–302. pmid:16510521; PubMed Central PMCID: PMC1446084

54. Murray AW, Szostak JW. Chromosome Segregation in Mitosis and Meiosis. Annual Review of Cell Biology. 1985;1(1):289–315. pmid:3916318

55. Farcas A-M, Uluocak P, Helmhart W, Nasmyth K. Cohesin's Concatenation of Sister DNAs Maintains Their Intertwining. Mol Cell. 2011;44(1–3):97–107. pmid:21981921; PubMed Central PMCID: PMC3240746

56. Wang LH-C, Mayer B, Stemmann O, Nigg EA. Centromere DNA decatenation depends on cohesin removal and is required for mammalian cell division. Journal of Cell Science. 2010;123(5):806–13. pmid:20144989

57. Kenney RD, Heald R. Essential roles for cohesin in kinetochore and spindle function in Xenopus egg extracts. Journal of Cell Science. 2006;119(24):5057–66. pmid:17158911

58. Baxter J, Sen N, Martinez VL, De Carandini MEM, Schvartzman JB, Diffley JFX, et al. Positive Supercoiling of Mitotic DNA Drives Decatenation by Topoisomerase II in Eukaryotes. Science. 2011;331(6022):1328–32. pmid:21393545

59. Piskadlo E, Oliveira RA. A Topology-Centric View on Mitotic Chromosome Architecture. Int J Mol Sci. 2017;18(12):2751. pmid:29258269; PubMed Central PMCID: PMC5751350

60. Nehlig A, Molina A, Rodrigues-Ferreira S, Honoré S, Nahmias C. Regulation of end-binding protein EB1 in the control of microtubule dynamics. Cell Mol Life Sci. 2017;74(13):2381–93. pmid:28204846

61. Ye AA, Verma V, Maresca TJ. NOD is a plus end–directed motor that binds EB1 via a new microtubule tip localization sequence. J Cell Biol. 2018;217(9):3007–17. pmid:29899040; PubMed Central PMCID: PMC6122986

62. Karg T, Warecki B, Sullivan W. Aurora B–mediated localized delays in nuclear envelope formation facilitate inclusion of late-segregating chromosome fragments. Mol Biol Cell. 2015;26(12):2227–41. pmid:25877868; PubMed Central PMCID: PMC4462941

63. Warecki B, Sullivan W. Micronuclei formation is prevented by Aurora B-mediated exclusion of HP1a from late-segregating chromatin in Drosophila. Genetics. 2018;210(1):171-187. pmid:29986897; PubMed Central PMCID: PMC6116970

64. Warecki B, Ling X, Bast I, Sullivan W. ESCRT-III–mediated membrane fusion drives chromosome fragments through nuclear envelope channels. Journal of Cell Biology. 2020;219(3):e201905091. pmid:32032426; PubMed Central PMCID: PMC7054997